Supported $Ir_xRu_{1-x}O_2$ Anode Catalysts for PEM-Water Electrolysis[×]

N. Baumann[1]*, C. Cremers[1], K. Pinkwart[1], J. Tübke[1]

[1] Fraunhofer-Institut für Chemische Technologie ICT, Joseph-von-Fraunhofer-Strasse 7, D-76327 Pfinztal, Germany

[*] Corresponding author, nils.baumann@ict.fraunhofer.de

Abstract

Since PEM-water electrolysis (PEMWE) produces very pure H_2, reacts fast and well to dynamic load conditions and is technologically simple, it could play a large role in a future hydrogen economy. One way to alleviate the drawback of expensive noble metal catalysts is to disperse the active component on a support. Tungsten oxide and tungsten carbide were investigated here comparing different synthesis routes. Adam's Fusion and hydrolysis route with the addition of support during different stages of the synthesis and mechanical mixing of catalyst and support were investigated and compared. Rotating Disk Electrode (RDE) measurements show high currents for mechanically mixed samples and samples obtained via hydrolysis with a WO_3 precursor. Single cell tests confirm catalyst activity and stability. Further studies are needed to completely understand catalyst behavior, especially fast activity loss during RDE.

Keywords: Degradation, Iridium, Mixed Oxide, Oxygen Evolution Reaction, Ruthenium, Supported Catalysts, Tungsten, Water Splitting

1 Introduction

Due to environmental concerns, the energy economy of the future has to move away from fossil fuels towards a renewable alternative. A very promising approach is based on H_2 as secondary energy carrier. If a renewable source of electricity, e.g. photovoltaics, wind turbines or hydroelectric power, is available, PEM-water electrolysis (PEMWE) can produce very pure H_2. PEMWE is also technologically relatively simple and reacts well to dynamic load conditions. [1] This is especially important when considering the dynamic nature of renewable electricity. H_2 can then be stored and transported easily. Fuel Cells can finally reconvert H_2 to electricity for stationary or mobile applications. The main disadvantage though is the high overpotential of the anode reaction (oxygen evolution reaction, OER) and the resulting harsh conditions, making the use of noble metal catalysts necessary. Additionally these conditions restrict the use of other materials at the anode. For example flow fields / bipolar plates are usually made of Ti [2, 3], which is sometimes covered with a thin Au layer [4, 5] to increase electronic conductivity and stability, as Ti easily forms Ti oxides with a much higher ohmic resistance, hindering cell performance.

Using support materials to reduce the catalyst loading is a common way to address the high costs of noble metal catalysts. [6] In case of the OER catalyst much research has focused on adding non-active metal oxides to the active component to form a mixed oxide in order to increase stability. [7 - 9] Probably the most frequently used material is SnO_2. [2, 4, 7, 10 – 12] The usual approach of using carbonaceous supports that serve as physical structures for dispersion and adhesion of active component cannot be applied here as the harsh conditions at the anode (high potentials and oxygen atmosphere) would corrode the carbon material and thus degrade the catalyst layer. Recently more research is being conducted to find a suitable support material for the OER catalyst that does not form a mixed oxide. Some examples include TaC, [13] antimony-doped tin oxide [14, 15] and TiC. [16] Besides offering a large surface area for good dispersion of active component the support has to be stable at the employed conditions and have a good electronic conductivity. Many transition metal oxides are stable at these conditions in addition of low cost. These characteristics are good for support materials. In contrast, they suffer from low electronic conductivity. If a sufficiently high loading of catalyst on these supports is used, this characteristic is not necessarily a limiting factor. Mazúr et al. [17] and Fuentes et al. [18] for example showed an improvement of TiO_2 supported IrO_2 catalysts, if 60 wt.-% IrO_2 are used. Another way to deal with the low electronic conductivity of oxide supports is to dope them in order to increase conductivity. Improved

[×] Presented at the FDFC conference, Toulouse / France, February 2015

activity has been shown for example by Oh et al. [14] for antimony doped tin oxide (ATO) and by Puthiypura et al. [5, 19] for ATO and indium doped tin oxide (ITO). Tungsten oxide was successfully used as catalyst support for methanol oxidation in fuel cells by Perchthaler et al. [20], although the authors indicate that they used substoichiometric oxides with a higher electronic conductivity than pure WO_3. More examples of use of WO_3 and WC as catalyst support material for example for methanol oxidation, oxygen reduction or CO oxidation can be found in a review about catalyst supports by Sharma et al. [6].

Motivation of this work was the development of anode catalysts for the so called HyCon system. [1] In brief, this is a directly coupled multijunction solar cell and PEM-water electrolysis cell. The solar cell is fitted with a Fresnel lens that focuses incoming sunlight on a small PV cell based on GaInP and GaInAs. The anode side of the electrolysis cell is in direct electrical and thermal contact with the PV cell, increasing technical simplicity and decreasing loss through cables and DC/DC converter. Due to long lifetime of the PV cell, the electrolysis cell has to be optimized for high stability at the given operating point.

In this work a mixed oxide of IrO_2 and RuO_2 has been synthesized with the theoretical stoichiometry of 1:1. WC and WO_3 have been chosen as support materials, as they are stable at high potentials and in oxygen atmosphere. Different synthesis routes were compared to achieve the best dispersion of active component and good binding of active component to support. Physical and electrochemical characterization of the supported catalysts was carried out.

2 Experimental

All chemicals were used as received. All ultrapure water used in synthesis and washing was ultrapure H_2O with a maximum of 0.055 $\mu S\ cm^{-1}$ unless mentioned otherwise.

2.1 Adam's Fusion

According to the Adam's Fusion synthesis protocol [10] $RuCl_3$ and $IrCl_3$ (both Alfa Aesar) with a molar ratio of 1:1 and a large excess (approximately tenfold) of $NaNO_3$ (Alfa Aesar) were stirred vigorously for 2 h in 2-Propanol (Carl Roth) at approximately 70°C solution temperature. After the liquid had evaporated the solid was calcined in a muffle furnace (KLS 07/11/M, Thermconcept, Bremen, Germany) in air atmosphere at 500°C for 30 min with the temperature being reached by a heating rate of 5 °C min^{-1}. Following cooling to room temperature the solid was washed extensively with ultrapure H_2O and filtered off using a 589[3] Blue Ribbon filter (Schleicher & Schuell GmbH, Dassel, Germany. $Ir_{0.5}Ru_{0.5}O_2$ was synthesized without support as reference material. WO_3 was synthesized from WC (H.C. Starck GmbH, Goslar, Germany) at 500°C for 5 h with the temperature being reached by a heating rate of 5°C min^{-1}. WC or WO_3 was added to the Adam's Fusion synthesis during the stirring phase or after drying the solid before calcination.

2.2 Hydrolysis

$IrCl_3$ and $RuCl_3$ were mixed in a 1:1 molar ratio and hydrolyzed in 0.2 M NaOH (Carl Roth) at 80°C for 1.5 h under stirring. Subsequently the solution was adjusted to pH 6 using concentrated HNO_3 (VWR) and stirred at 80°C for another hour. After filtration (same filter as above) of the metal hydroxides the mixture was calcined in air atmosphere either at 600°C for 30 min or 400°C for 4 h with the temperatures being reached by a heating rate of 5°C min^{-1}. [9] WC or WO_3 support was added during the hydrolysis step, after the solution pH was adjusted or after drying and before calcination.

2.3 Hydrolysis with Ammonium Paratungstate (APT)

The same hydrolysis procedure as in Section 2.2 was conducted. Following, the dried metal hydroxides were mixed with $(NH_4)_{10}(H_2W_{12}O_{42})$ * 4 H_2O (ammonium paratungstate, APT) (Alfa Aesar) in the molar ratio of 1:9 and vigorously stirred in ultrapure H_2O for 4 h. Calcination of dried mixture was carried out in air atmosphere at 400°C for 4 h with the temperature being reached by a heating rate of 5°C min^{-1}. [21]

2.4 Mechanical Mixing of Catalyst and Support

$Ir_{0.5}Ru_{0.5}O_2$ was synthesized according to Adam's fusion method. Catalyst powder and support were mechanically mixed before ink preparation. In case of the WO_3 the catalyst / support mixture was annealed at 200°C for 2 h under air or N_2 atmosphere in a tube furnace (HST-12/400, Carbolite, Hope,

United Kingdom). Another approach included preparing separate inks of catalyst and support and mixing them afterwards.

2.5 Physical Characterization

X-ray diffracton (XRD) measurements were taken with a Diffraktometer D8 Series2 (Bruker AXS, Billerica, MA, USA). Transmission electron microscopy (TEM) imaging was done at Fraunhofer-ICT-IMM (Mainz, Germany). X-ray photoelectron spectroscopy (XPS) analysis was done by Fraunhofer-IWM (Pfinztal, Germany) using a PHI 5000 VersaProbe instrument (Ulvac-Phi, Inc., Chigasaki, Japan). Catalyst powder was pressed into an In-foil using a spatula. Samples were excited by monochromatic $Al_{K\alpha}$ (1486 eV) radiation, reflected by a quartz crystal. Samples were scanned in 10^{-7} Pa vacuum with 50 W excitation energy. The X-ray beam had a diameter of 200 mm and was scanned over a 200 µm x 300 µm area. The elements were quantified using peak area and Multipeak software with default standard factors. Scanning electron microscopy (SEM) / energy dispersive X-ray spectroscopy (EDX) imaging was performed in house using EVO MA10 SEM (Zeiss, Oberkochen, Germany) with X-Max EDX (Oxford Instruments, Abingdon, UK). Conductivity of powder WO_3 was measured at Leibniz Institute for Polymer Research, Dresden, Germany by Dr. Jürgen Pionteck. Maximum electronic conductivity of three samples was measured at increasing pressures up to 30 MPa and averaged.

2.6 Rotating Disk Electrode (RDE) Measurements

Electrochemical investigation was carried out using a Modulated Speed Rotator RDE setup (Pine Research Instrumentation, Durham, NC, USA) with 5 mm diameter glassy carbon disk electrode (GCE). The catalyst was dispersed in a 1 : 1 ultrapure H_2O : ethanol (Merck) mixture with a concentration of 1 mg mL^{-1}. In order to homogenize the ink, it was subjected to ultrasonication using T 570/H sonicators (Elma Schmidbauer GmbH, Singen, Germany) with operating frequency of 35 kHz. The ultrasonic power was determined as described by Pollet [22] using ultrapure H_2O. A measured mass of water was subjected to ultrasonication and the solution temperature was recorded every 5 s for 1 minute using Fluke 289 True RMS Multimeter (Fluke, Everett, WA, U.S.A.). The data was fitted with sixth-order polynomial function. Ultrasonic power (P_T) was determined using specific heat capacity (C_p) of water (4.184 J g^{-1} K^{-1}) [22] and mass (m) of water according to Equation (1).

$$P_T = m \times C_p \times (dT/dt)_{t=0}$$

Following 30 min of homogenization, 10 µL of the ink was pipetted onto the glassy carbon disk. After the electrode had been dried 10 µL of 0.01 wt.-% polytetrafluoroethylene (PTFE) (in ultrapure H_2O) was pipetted on top as binder. RDE measurements were conducted in 0.5 M H_2SO_4 (Merck) with Pt-wire counter electrode, reversible hydrogen electrode (RHE) (Gaskatel GmbH, Kassel, Germany) reference electrode and SP-300 potentiostat (Bio-Logic SAS, Claix, France). The solution was deaerated with Ar at least 15 min prior to and during all measurements. Activity for oxygen evolution was studied by cyclic voltammetry between 1.2 V and 1.7 V *vs.* RHE with a scan rate of 10 mV s^{-1}.

2.7 Single Cell Tests

Catalyst ink was prepared with 25 wt.-% ethanol in ultrapure H_2O. Catalyst and support were individually homogenized ultrasonically (same conditions as described above), then combined and further homogenized. Afterwards the ink was stirred 2 days. Finished ink was sprayed onto Nafion 115 membrane, which was heated to 60 °C, with a loading of 2.58 mg cm^{-2} $Ir_{0.5}Ru_{0.5}O_2$ and 2.74 mg cm^{-2} WO_3 (1:1) or 1.91 mg cm^{-2} $Ir_{0.5}Ru_{0.5}O_2$ and 17.15 mg cm^{-2} WO_3 (1:9). 13.08 wt.-% Nafion based on the total catalyst / support mass was used as binder. Sigracet 35 BC (SGL Carbon, Wiesbaden, Germany) or Freudenberg H2315 (Freudenberg, Weinheim, Germany) was coated with 40 wt.-% Pt / Vulcan (Alfa Aesar) ink (6 mg cm^{-2}). Membrane electrode assemblies (MEAs) were tested in a cF 25/100 cell fixture (Baltic FuelCells GmbH, Schwerin, Germany) with Ti flow fields, Ti-fleece anode porous transport layers (PTLs) and Pt / C coated Sigracet 35 BC cathode PTLs. Distilled H_2O was pumped through at both electrodes using peristaltic pumps; at the cathode with around 2 mL min^{-1} at the anode with varying flow rates. HCP-803 potentiostat with 80 A booster (Bio-Logic SAS, Claix, France) was used for the single cell tests. For comparison a commercial MEA (catalyst coated membrane) was measured in the same set-up. This consisted of Fumea EF-50 MEA (FuMA-Tech, Bietigheim-Bissingen, Germany) with Ir-based anode, Pt-based cathode and PTFE reinforced membrane with 360 µm thickness. Ti-fleece anode PTL and Sigracet 35 BC cathode PTL were used.

3 Results and Discussions

RuO_2 is the most active known material for the oxygen evolution reaction, but is prone to oxidization at high potentials. [23] Formation of a mixed oxide with IrO_2, which is less active for the oxygen evolution reaction, but more stable, stabilizes the RuO_2. Oxidation of WC to WO_3 was confirmed by XRD in addition to the conspicuous light yellow color of WO_3.

3.1 Adam's Fusion

Formation of mixed oxide of $Ir_xRu_{1-x}O_2$ in the rutile structure was confirmed via XRD, see Figure 1.

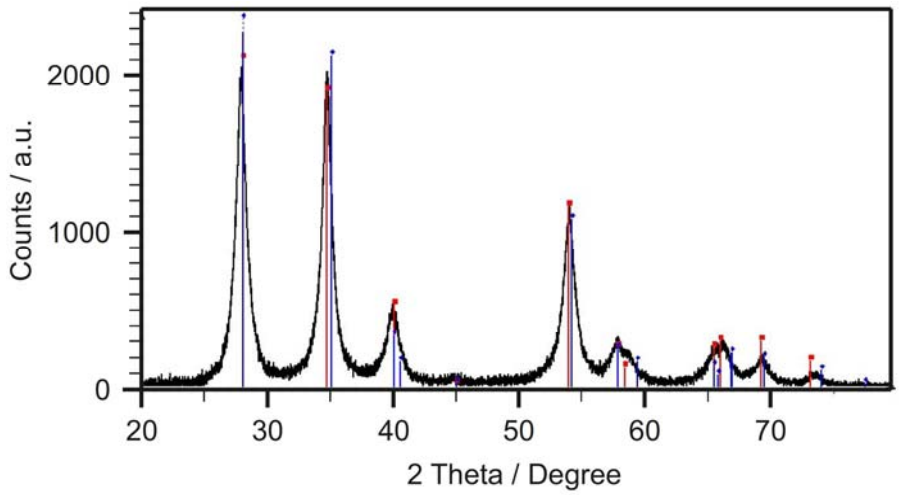

Figure 1: XRD of $Ir_{0.5}Ru_{0.5}O_2$. Red and blue reflections correspond to IrO_2 and RuO_2 respectively.

Since RuO_2 and IrO_2 have the same structure with similar crystal parameters they easily form a mixed oxide. Throughout this work $Ir_{0.5}Ru_{0.5}O_2$ is used, in full knowledge that it is the theoretical value and there is likely some variation in the exact composition. Addition of WC or WO_3 resulted in a large loss of material after washing. This is believed to be due to formation of tungsten nitrosyls and or chloro-complexes. It is well known that transition metals form a variety of complexes with nitrosyls and chloro ligands [24] and $NaNO_3$ gives of nitrous oxide during reaction with metal chlorides according to Equation (2).

$$MeCl_3 + 3\ NaNO_3 \rightarrow MeO_2 + 3\ NaCl + 3\ NO_2 \uparrow + \tfrac{1}{2}\ O_2 \uparrow \quad (2)$$

These tungsten complexes probably evaporated during the synthesis or were washed out afterwards. XPS results back this assumption, as only 2.19 wt.-% of W was detected in the dried sample.

3.2 Hydrolysis

Due to the problem of NO_x being generated by $NaNO_3$, the synthesis was changed to include no additional oxygen donor. Successful hydrolyzation of $RuCl_3$ and $IrCl_3$ was visible from a dark blue color of the solution. For the addition of WC as support a calcination temperature of 400°C was chosen, as it lies below the oxidation temperature of WC. However, after 4 h at 400°C in oxygen atmosphere the WC was still completely oxidized. There are varying reports for the oxidation temperature of WC, e.g. Kurlov et al. investigated the influence of particle size on oxidation temperature. [25] Considering the long calcination time of 4 h even a temperature close to the oxidation temperature will result in complete oxidation of WC. It was observed that adding WO_3 before the acidification step leads to reaction with NaOH to form sodium paratungstate according to Equation (3), which was confirmed via XRD.

$$WO_3 + 2\ NaOH \rightarrow Na_2WO_4 + H_2O \quad (3)$$

This is undesirable for two reasons. Firstly, Na_2WO_4 has a high solubility in water, thus most of the support is washed out during synthesis. Absence of pale yellow color of WO_3 in the finished supported

catalyst supports this claim. Secondly, it brings sodium ions into the catalyst mixture, which might pose a problem during electrolysis operation, e.g. catalyst poisoning and decrease of membrane ionic conductivity due to substitution of protons with Na^+ ions.

However, if WO_3 is added after the acidification step it does not react. As was expected, calcining the metalhydroxides without $NaNO_3$ did not result in a loss of material, supporting the hypothesis of tungsten complexes forming during the Adam's fusion reaction.

3.3 Hydrolysis with APT

Formation of WO_3 during the calcination step was well visible from the pale yellow color of WO_3 in the finished catalyst. XRD was used again to prove the formation of WO_3.

3.4 Mechanical Mixing of Catalyst and Support

Some inhomogeneity was visible for the WO_3 supported sample when mechanically mixed. The pale yellow color, in contrast to the black oxide catalyst, makes it easily visible if the support and the catalyst are not homogeneously mixed. Since the catalyst and support were only mixed in a mortar, this is not surprising. However, homogeneity can easily be improved by dispersing the support and catalyst in a solvent and either stirring the dispersion or subjecting it to an ultrasonication treatment.

3.5 Physical and Electrochemical Characterization

Prepared inks showed homogeneous dispersion after the sonication treatment. Particles were consequently well distributed on the glassy carbon disk electrode. It has been studied by some research groups that the quality of the ink depends on the ultrasonication treatment. Pollet et al. [26] for example investigated the effect of different ultrasonication frequency, power and duration on Pt/C inks. They showed that best results were obtained from sonication between 30 min and 120 min. The 60 minutes used here lie in this range. Ultrasonication power, as determined according to method described by Pollet [22], was 8.3 W (average of three measurements), which is a typical value for ink homogenization. It was also observed with our inks that an ultrasonication time of less than 30 minutes resulted in poor homogenization. The authors also showed that different inks have different optimum sonication parameters. A detailed investigation of ink quality and sonication treatment was however outside the scope of the work presented here. Figure 2 shows the first scan of the RDE measurements for the different catalysts. The current is normalized to the theoretical amount of active component, i.e. $Ir_{0.5}Ru_{0.5}O_2$ in case of the supported catalysts.

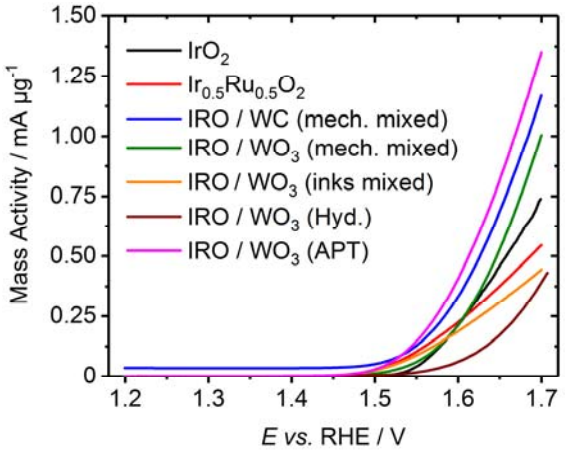

Figure 2: First scan of the OER activity of differently synthesized catalysts. For reasons of limited space $Ir_{0.5}Ru_{0.5}O_2$ was abbreviated as IRO in the Figure legend. All measurements contain 10 wt.-% $Ir_{0.5}Ru_{0.5}O_2$, except the sample with mixed inks (orange), which contains 50 wt.-% $Ir_{0.5}Ru_{0.5}O_2$.

All catalysts were prepared on 5 mm diameter glassy carbon electrodes and the theoretical total loading (catalyst and support) was 10 µg. Values for unsupported catalyst and IrO_2 (Alfa Aesar) are shown as reference. Due to limited space in the diagram, the mixed oxide is abbreviated as IRO in the Figure legend. All samples contain 10 wt.-% active component, except the sample with mixed inks (orange line), which contains 50 wt.-% active component. Onset potential for OER and maximum current

density (at 1.7 V) for all samples are summarized in Table 1. The values for the onset potential are close together with the exception of a slightly higher value for the commercial IrO_2 and the $Ir_{0.5}Ru_{0.5}O_2$ / WO_3, where the WO_3 was added after the hydrolyzation step. It is not entirely clear at this point what the reasons for these differences are. Probably the onset potential depends on the exact morphology of the catalyst, which is different for the samples. In any case, the effect is not too strong and the more important value is the activity at higher potentials, where commercial electrolyzers are operated.

Table 1: Electrochemical characteristics of samples measured via RDE.

Sample	**Onset potential / V**	**Maximum current density / mA µg^{-1}**
IrO_2	1.53	0.738
$Ir_{0.5}Ru_{0.5}O_2$	1.47	0.545
IRO / WC (mech. mixed)	1.49	1.17
IRO / WO_3 (mech. mixed)	1.49	1.00
IRO / WO_3 (inks mixed)	1.47	0.445
IRO / WO_3 (Hyd.)	1.53	0.391
IRO / WO_3 (APT)	1.47	1.35

The 10 wt.-% $Ir_xRu_{1-x}O_2$ / WO_3 catalyst synthesized with the APT approach shows the highest current. XPS measurements of the APT sample are shown in Figure 3. Peaks correlate well with the respective oxides, as is true for all investigated samples. Atomic distribution of 8.5 % Ru, 19.0 % Ir and 72.5 % W revealed a real loading of 27.5 at.-% (24.3 wt.-%) active component. This can explain the higher current, as more active component is available than the calculated 10 wt.-% for the diagram.

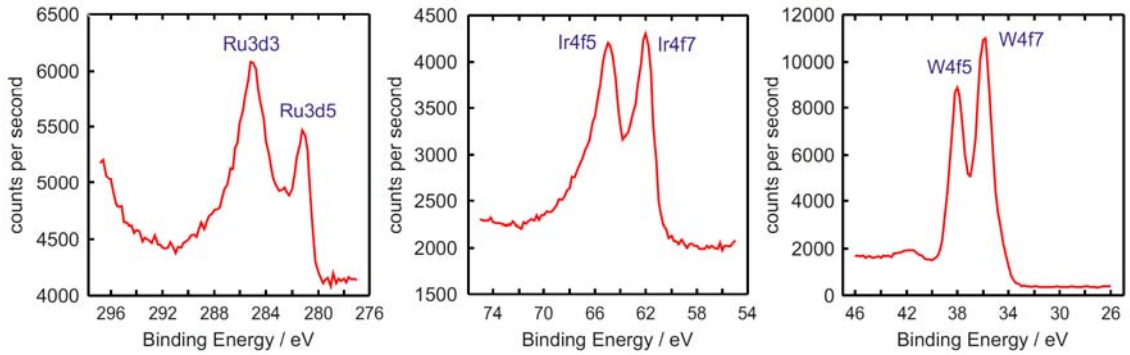

Figure 3: XPS peaks of $Ir_{0.5}Ru_{0.5}O_2$, APT approach.

During the calcination step this sample was held at 400°C for 4 h, which could explain the low Ru content, as RuO_2 is not so stable and the calcination temperature might have been too low to form a complete mixed oxide of IrO_2 and RuO_2. TEM image of 10 wt.-% $Ir_{0.5}Ru_{0.5}O_2$ / WO_3 (APT approach) shows formation of needle like structures of the support, Figure 4.

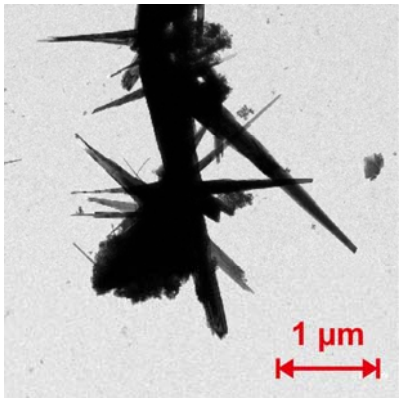

Figure 4: TEM image of 10 wt.-% $Ir_{0.5}Ru_{0.5}O_2$ / WO_3, APT approach.

This might constitute a problem, as it is conceivable that these needles puncture the membrane during MEA fabrication (e.g. during spraying of catalyst onto membranes) or during compression of the MEA in the cell. Consequently such mechanical damage to the membrane might lead to cell failure. Additionally the catalyst particles are not well bound to the support.

Both mechanically mixed catalyst and support show high activity as well. XPS results give atomic distribution of 5.0 % Ru, 6.5 % Ir and 88.5 % W for the WO_3 sample annealed in N_2, being very close to the theoretical composition (9.35 wt.-%). In addition, the TEM images of a sample annealed in air instead of N_2 show good binding of catalyst particles to the support, with individual catalyst particles being around 5 nm big, see Figure 5. Atomic distribution of the sample annealed in air showed higher catalyst percentages, namely 6.3 % Ru, 15.7 % Ir and 78.0 % W (19.48 wt.-% active component). This lower part of Ru in relation to Ir suggests that it is advantageous to anneal the catalyst in N_2 to minimize the danger of RuO_2 oxidation and loss. It has to be noted that XPS is very surface sensitive (about 1 nm sampling depth) and some of the elemental distribution might be explained by migratory effects. Ir enrichment at the surface of a mixed Ir-Ru oxide for example was reported by Owe et al. [9]

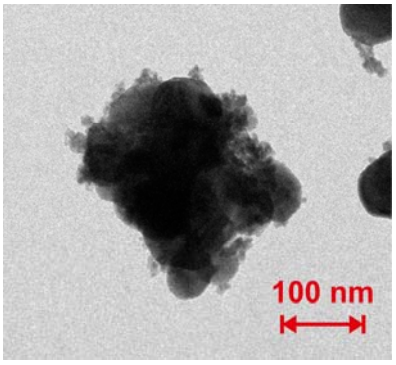

Figure 5: TEM image of 10 wt.-% $Ir_{0.5}Ru_{0.5}O_2$ / WO_3 mechanically mixed and annealed in air.

The sample, where WO_3 support was added after the acidification step during hydrolysis procedure resulted in a fairly low OER activity. Considering an atomic distribution of only 1.0 % Ru, 5.4 % Ir and 93.6 % W, with an overall active component percentage of 6.4 at.-% (5.84 wt.-%), the current in Figure 2 should be a little higher; as it was calculated with 10 wt.-%. TEM images show partly large agglomerates of support and catalyst particles (Figure 6).

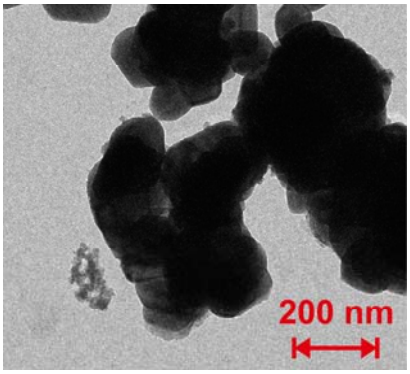

Figure 6: TEM image of 10 wt.-% $Ir_{0.5}Ru_{0.5}O_2$ / WO_3 mixed after the acidification step during hydrolysis synthesis.

Moreover, the catalyst particles are not well bound to the support material, but were observed in part as agglomerates of around 100 nm size. TEM images of unsupported $Ir_xRu_{1-x}O_2$ (not shown) show mostly larger agglomerates, which would lead to a low electrochemical active surface area and could thus explain why the OER activity is lower than for commercial IrO_2, which in theory has a lower activity than mixed $Ir_xRu_{1-x}O_2$.

Preparing catalyst and support separately and mixing inks results in a rather low activity. Agglomerates and a poor binding of catalyst to support is probably responsible for these results, though has to be confirmed with further TEM imaging.

Figure 7 shows current at 1.7 V (*vs.* RHE) *vs.* cycle number during OER RDE measurements. As well as in Figure 2 the current is normalized to the theoretical amount of active component. Again, mixed oxide is abbreviated as IRO and all samples contain 10 wt.-% active component or 50 wt.-% in case of mixed inks (orange line).

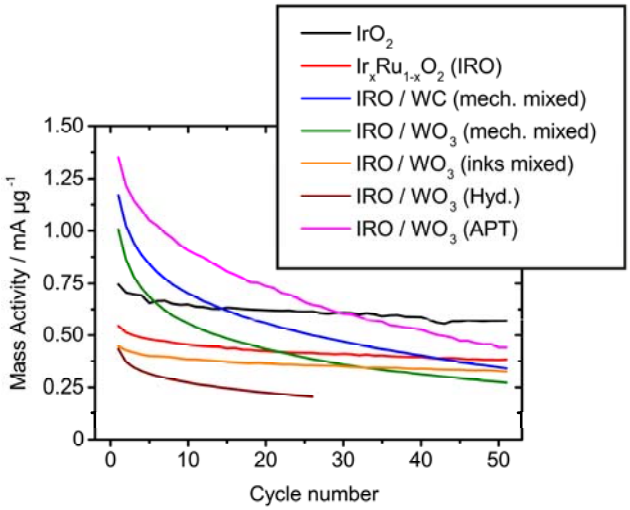

Figure 7: Change of current at 1.7 V *vs.* RHE with proceeding cycle number. For reasons of limited space $Ir_{0.5}Ru_{0.5}O_2$ was abbreviated as IRO in the Figure legend. All measurements contain 10 wt.-% $Ir_{0.5}Ru_{0.5}O_2$, except the sample with mixed inks (orange), which contains 50 wt.-% $Ir_{0.5}Ru_{0.5}O_2$.

Table 2 summarizes the degradation, which is given in loss of current density per cycle for the first 25 cycles, the second 25 cycles and the overall loss. It is important to note that these values represent an average degradation rate.

Table 2: Degradation characteristics of samples measured via RDE.

Sample	**Degradation rate (1-25) / mA µg-1 per cycle**	**Degradation rate (26-51) / mA µg-1 per cycle**	**Degradation rate (1-51) / mA µg-1 per cycle**
IrO_2	5.25×10^{-3}	1.76×10^{-3}	3.41×10^{-3}
$Ir_{0.5}Ru_{0.5}O_2$	5.21×10^{-3}	1.23×10^{-3}	3.17×10^{-3}
IRO / WC (mech. mixed)	26.41×10^{-3}	6.31×10^{-3}	16.23×10^{-3}
IRO / WO_3 (mech. mixed)	26.18×10^{-3}	4.83×10^{-3}	15.36×10^{-3}
IRO / WO_3 (inks mixed)	3.57×10^{-3}	1.21×10^{-3}	2.34×10^{-3}
IRO / WO_3 (Hyd.)	8.88×10^{-3}	-	8.66×10^{-3}
IRO / WO_3 (APT)	27.65×10^{-3}	8.27×10^{-3}	17.87×10^{-3}

As can be seen in Figure 7, the degradation behavior is by no means linear and the fastest degradation takes place in the beginning. This is also evident in Table 2, where the degradation rate during the second 25 cycles is in all cases smaller than the initial degradation. It is well visible that all catalysts that have a high current also show a fast degradation. After 50 cycles the activity has dropped by more than 60 % for the APT approach and the mechanically mixed catalyst and support. It is not clear what is causing this rapid drop in OER activity. Visual inspection (digital microscope) shows no major material loss after RDE cycling. However, contact of the catalyst to the GCE surface might be lost during the measurements, yet dissolution of particles prevented by the PTFE layer on top of the electrode. Considering that the unsupported $Ir_{0.5}Ru_{0.5}O_2$, IrO_2 and $Ir_{0.5}Ru_{0.5}O_2$ / WO_3 hydrolysis route show a lower degradation rate, the reason for the high degradation rate for the supported catalysts could be a low adhesion of WO_3 / WC on glassy carbon. In all samples with high support content, a considerable amount of support is in contact

with the glassy carbon. If the adhesion is not good, the support will be lost during the RDE cycling and consequently all active component bound to the support particle. Formation of inactivating adsorbate layers might also be a reason to explain the activity loss. Sulphate ions are known to adsorb on metal and metaloxide surfaces and poison catalytic activity. Further studies need to address this issue and be tailored to find out what is causing this activity loss.

3.6 Single Cell Tests

Catalyst and support were uniformly distributed on the whole MEA, as confirmed by SEM / EDX elemental mapping. Figure 8 shows current density of subsequent potentiostatic measurements using MEA with 50 wt.-% $Ir_{0.5}Ru_{0.5}O_2$ / WO_3 at 1.9 V and 25 °C. Note that measurements had different lengths, ranging from 10 min to 3 h. Note also that the current density was calculated from the geometric area of the MEA.

The MEA goes through an initial activation phase, as is commonly observed with fuel cells and electrolyzers. [27, 28] It takes about 21 h of running time to reach the maximum performance of approximately 110 mA cm^{-2}. This is rather long, but still lies in the commonly observed time range (up to 48 h). After reaching the maximum performance the MEA loses some activity over the next hours and stabilizes at around 100 mA cm^{-2} after approximately 33.4 h. Comparing the single cell performance to the RDE measurements shows a much larger stability in single cell tests. This result points to a problem other than catalyst degradation for the activity loss during RDE measurements. In case of the MEAs distilled H_2O was used, instead of H_2SO_4 in the RDE setup, hence the effect of sulphate ion adsorption is not present here. Moreover, Nafion was used as binder, instead of PTFE.

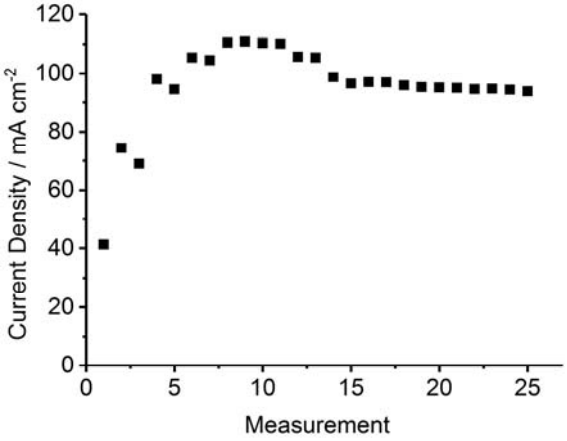

Figure 8: Current densities during different measurements of MEA at 1.9 V.

For comparison a commercial MEA from FuMA-Tech was measured at the same conditions. Current density at 1.9 V and 25 °C was approximately 400 mA cm^{-2} for the commercial single-cell, being a factor of almost 4 higher than the cell with novel WO_3 supported $Ir_{0.5}Ru_{0.5}O_2$ catalyst. It has to be noted that many details like exact catalyst composition and loading as well as binder content are not known for the commercial MEA. Direct comparison between the two cells consequently has to be evaluated carefully. For more detailed comparison between a commercial cell and novel supported catalyst, please refer to our previous paper. [29]

SEM / EDX elemental mapping after these measurements shows still uniform distribution of catalyst and support. This confirms the stability of the catalyst, Figure 9. Black lines well visible in the lower right corner of the images are regions where the catalyst has been lost. As all catalyst constituents show the same loss in these areas, it is concluded that this loss is due to mechanical delamination, happening when the Ti-fleece is removed at the disassembly of the cell. The shape of the delaminated area further supports this conclusion, since it correlates well with the size and shape of the individual Ti-fleece fibers. It is possible that these lines originated from cracks formed in the catalyst layer during deposition. However, post-mortem EDX of other samples (not shown) on Nafion membranes did not show these lines. Moreover, yet another sample with a different porous transport layer showed black lines corresponding to the respective fiber size and shape (post-mortem). Third, there were no visible cracks in the catalyst layer after spraying and the MEA appeared uniform to the naked eye. In light of these results the hypothesis of

cracks forming in the catalyst layer during hot-spraying was dismissed. Future EDX mapping of a MEA prior to measurements is planned to confirm this.

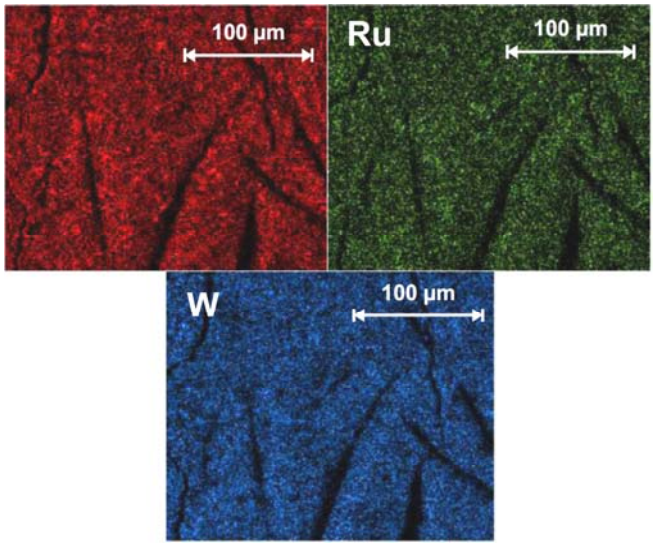

Figure 9: SEM / EDX mapping of MEA anode side after measurements.

In order to investigate the effect of the ratio of active component to support, a MEA with only 10 wt.-% $Ir_{0.5}Ru_{0.5}O_2$ / WO_3 was prepared. Figure 10 shows the current density *vs.* time of the respective MEA during chronoamperometric measurement at 1.9 V and 25 °C.

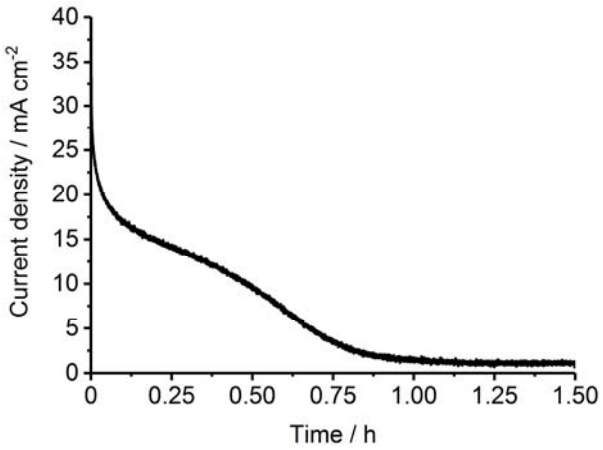

Figure 10: Current density measurement *vs.* time of MEA with 10 wt.-% $Ir_{0.5}Ru_{0.5}O_2$ / WO_3 at 1.9 V and room temperature.

Not only does the cell show a much lower current density compared to the cell with 50 wt.-% catalyst (only approximately 20 mA cm^{-2} *vs.* 42 mA cm^{-2}), but it also loses its activity relatively fast, dropping to almost zero activity within 1 hour. Although the loading of active component was a little lower (1.91 mg cm^{-2} *vs.* 2.58 mg cm^{-2}), it is still lower than the cell with higher percentage active catalyst. The most likely explanation for the low activity is the very low electronic conductivity of WO_3, which was measured only at 2.92 x 10^{-6} S cm^{-1}, which is far below the values reported in the literature, which are on the order of 10^{-4} S cm^{-1}. [30, 31] Measured electronic conductivity depends strongly on the preparation and measurement conditions and small particle sizes, leading to large ohmic losses at grain boundaries could explain these results. The reason for the fast degradation is currently not understood, but efforts are being undertaken to find out what is causing this fast loss in activity. For more detailed measurements of these supported catalysts and ways to try to increase electronic conductivity and activity, see our previous paper. [29]

4 Conclusions

Several synthesis routes to obtain WO_3 or WC supported $Ir_{0.5}Ru_{0.5}O_2$ have been compared. Judging from RDE measurements the hydrolysis route including APT as WO_3 precursor and mechanical mixing of catalyst and support followed by annealing show the best performances according to initial current. During RDE measurements these catalysts also show the highest degradation rate. At this point it is not clear what is causing this activity drop.

Due to the formation of needle shaped support particles during the synthesis following the APT approach and considering the results from XPS measurements, it can be concluded that mechanical mixing of support and catalyst followed by annealing under inert atmosphere offers the best route to WO_3 / WC supported $Ir_{0.5}Ru_{0.5}O_2$ catalysts. Single cell tests with mechanically mixed catalyst and support show stable performance for at least 39 h. Although current densities are relatively small, it is believed that a fine tuning of synthesis and MEA fabrication parameters will result in an increase of performance and stability.

Acknowledgments

Financial support by the German Federal Ministry of Education and Research (BMBF) under the contract number FKZ 03SF0432A is greatly acknowledged. Gratitude is also expressed to Harald Fietzek for help with XRD measurements, Eberhard Nold for help with XPS measurements and Raphael Thiermann for help with TEM imaging.

References

[1] S. Rau, S. Vierrath, J. Ohlmann, A. Fallisch, D. Lackner, F. Dimroth, T. Smolinka, *Energy Technol.* **2014**, *2*, 43-53.
[2] E. Mayousse, F. Maillard, F. Fouda-Onana, O. Sicardy, N. Guillet, *Int. J. Hydrogen Energy* **2011**, *36*, 10474-10481.
[3] L. Ma, S. Sui, Y. Zhai, *Int. J. Hydrogen Energy* **2009**, *34*, 678-684.
[4] J. Xu, G. Liu, J. Li, X. Wang, *Electrochim. Acta* **2012**, *59*, 105-112.
[5] V. K. Puthiyapura, M. Mamlouk, S. Pasupathi, B. G. Pollet, K. Scott, *J. Power Sources* **2014**, *269*, 451-460.
[6] S. Sharma, B. G. Pollet, *J. Power Sources* **2012**, *208*, 96-119.
[7] K. Kadakia, M. K. Datta, O. I. Velikokhatnyi, P. Jampani, S. K. Park, S. J. Chung, P. N. Kumta, *J. Power Sources* **2014**, *245*, 362-370.
[8] J. L. Corona-Guinto, L. Cardeño-García, D. C. Martínez-Casillas, J. M. Sandoval-Pineda, P. Tamoya-Meza, R. Silva-Casarin, R. G. González-Huerta, *Int. J. Hydrogen Energy* **2013**, *38*, 12667-12673.
[9] L.-E. Owe, M. Tsypkin, K. S. Wallwork, R. G. Haverkamp, S. Sunde, *Electrochim. Acta* **2012**, *70*, 158-164.
[10] X. Wu, J. Tayal, S. Basu, K. Scott, *Int. J. Hydrogen Energy* **2011**, *36*, 14796-14804.
[11] L. Vazquez-Gomez, S. Ferro, A. De Battisti, *Appl. Catal. B* **2006**, *67*, 34-40.
[12] T. A. F. Lassali, J. F. C. Boodts, L. O. S. Bulhões, *J. Non-Cryst. Solids* **2000**, *273*, 129-134.
[13] J. Polonský, P. Mazúr, M. Paidar, E. Christensen, K. Bouzek, *Int. J. Hydrogen Energy* **2014**, *39*, 3072-3078.
[14] H.-S. Oh, H. N. Nong, T. Reier, M. Gliech, P. Strasser, *Chem. Sci.* **2015**, *6*, 3321-3328.
[15] M. Thomassen, T. Mokkelbost, E. Sheridan, A. Lind, *ECS Trans.* **2011**, *35*, 271-279.
[16] S. Sui, L. Ma, Y. Zhai, *Asia-Pac. J. Chem. Eng.* **2009**, *4*, 8-11.
[17] P. Mazúr, J. Polonský, M. Paidar, K. Bouzek, *Int. J. Hydrogen Energy* **2012**, *37*, 12081-12088.
[18] R. E. Fuentes, J. Farell, J. W. Weidner, *Electrochem. Solid St.* **2011**, *14*, E5-E7.
[19] V. K. Puthiyapura, S. Pasupathi, H. Su, X. Liu, B. Pollet, K. Scott, *Int. J. Hydrogen Energy* **2014**, *39*, 1905-1913.
[20] M. Perchthaler, T. Ossiander, V. Juhart, J. Mitzel, C. Heinzl, C. Scheu, V. Hacker, *J. Power Sources* **2013**, *243*, 472-480.
[21] M. N. Alaya, M. A. Rabah, *Arabian Journal of Chemistry* http://dx.doi.org/10.1016/j.arabjc.2012.11.012
[22] B. G. Pollet, *Electrocatalysis* **2014**, *5*, 330-343.
[23] R. Kötz, S. Stucki, D. Scherson, D. M. Kolb, *J. Electroanal. Chem.* **1984**, *172*, 211-219.
[24] N. G. Connelly, *Inorg. Chim. Acta Rev.* **1972**, *6*, 47-89.
[25] A. S. Kurlov, A. I. Gusev, *Inorg. Mater.* **2011**, *47*, 133-138.
[26] B. G. Pollet, J. T. E. Goh, *Electrochim. Acta* **2014**, *128*, 292-303.

[27] Z. Xu, Z. Qi, C. He, A. Kaufmann, *J. Power Sources* **2006**, *156*, 315-320.
[28] X.-Z. Yuan, S. Zhang, J. C. Sun, H. Wang, *J. Power Sources* **2011**, *196*, 9097-9106.
[29] N. Baumann, C. Cremers, K. Pinkwart, J. Tübke, *Energy Technol.* **2016**, *4*, 212-220.
[30] P. R. Patil, P. S. Patil, *Thin Solid Films* **2001**, *382*, 13-22.
[31] K. Aguir, C. Lemire, D. B. B. Lollman, *Sens. Actuators B* **2002**, *84*, 1-5.